Individual patterns of functional connectivity in neonates as revealed by surfaced-based Bayesian modeling

Diego Derman[1], Damon D. Pham[2], Amanda F. Mejia[2], and Silvina L. Ferradal[1]

[1]Department of Intelligent Systems Engineering, Indiana University, USA
[2]Department of Statistics, Indiana University, USA

ABSTRACT

Resting-state functional connectivity is a widely used approach to study the functional brain network organization during early brain development. However, the estimation of functional connectivity networks in individual infants has been rather elusive due to the unique challenges involved with functional magnetic resonance imaging (fMRI) data from young populations. Here, we use fMRI data from the developing Human Connectome Project (dHCP) database to characterize individual variability in a large cohort of term-born infants (N = 289) using a novel data-driven Bayesian framework. To enhance alignment across individuals, the analysis was conducted exclusively on the cortical surface, employing surface-based registration guided by age-matched neonatal atlases. Using 10 minutes of resting-state fMRI data, we successfully estimated subject-level maps for fourteen brain networks/subnetworks along with individual functional parcellation maps that revealed differences between subjects. We also found a significant relationship between age and mean connectivity strength in nearly all brain regions, including previously unreported findings in higher-order networks. These results illustrate the potential advantages of surface-based methods and statistical approaches in uncovering individual variability within very young populations.

Keywords neonatology · brain development · fMRI · rs-fMRI · functional connectivity · resting-state networks · statistical methods · Bayesian modeling

Introduction

The human brain undergoes significant changes during late gestation and early infancy. Characterizing the functional brain organization during early postnatal ages is clinically relevant to elucidate how different genetic factors and environmental hazards may impact subsequent development. Resting-state functional connectivity (RSFC) is a widely used approach to delineate the functional brain organization in the perinatal period since subjects are imaged at rest without requiring the performance of any specific task. Typically, RSFC methods look for temporal coherence of spontaneous fluctuations of functional magnetic resonance imaging (fMRI) signals to define resting-state networks (RSNs), also known as the functional connectome. Seminal studies based on RSFC methods have shown that the functional connectome during early development is affected by premature birth (Doria et al., 2010; Smyser et al., 2010), maternal stress (DeSocio, 2018; Sandman et al., 2012), developmental dyslexia (Cao et al., 2014, Yu et al., 2022), and prenatal drug exposure (Merhar et al., 2021), among other factors. While these studies have provided important insights into the typical and atypical functional brain organization in early life, the vast majority has focused on the estimation of RSNs at the group level (i.e., derived from multi-subject data). In recent years, it has been shown that the functional connectome is associated with later cognitive and behavioral outcomes (He et al., 2018). Therefore, individual characterizations are critical to make subject-based predictions of clinical relevance.

The robust estimation of RSNs in individual infants has been rather elusive due to the inherently low signal-to-noise ratio (SNR) of the resting-state fMRI data and the unique sources of noise (e.g. idiosyncratic head motion, faster cardiac and respiration rates) in this population (Smyser and Neil, 2015). Traditional RSFC analysis approaches like independent component analysis (ICA) produce clean estimations of RSNs when combining data from a large number of infants (Eyre et al., 2021; Gao et al., 2015) but fail to capture individual differences. In contrast, estimations of subject-level RSNs obtained from methods such as dual regression have low power to mitigate noise from single-subject data. The robustness of individual estimations can be also improved by increasing the scan duration, as shown by RSFC studies in healthy adults (Birn et al., 2013; Laumann et al., 2015, Gordon et al., 2017). However, this approach is rarely practical or cost-effective when considering infant and clinical populations.

In this study, we explore Bayesian modeling in combination with surface-based analysis to improve individual estimations of RSNs in infants during the first weeks of life. The proposed Bayesian framework (Mejia et al., 2020) requires population priors or templates, so we leverage the information contained in the large open-access dataset from the developing Human Connectome Project (dHCP) (Edwards et al., 2022). A critical assumption of the Bayesian framework is that all the subjects are anatomically co-registered to a common atlas space. Thus, to optimize the anatomical alignment across individuals with different gestational ages, the analysis is entirely done on the cortical surface using registration techniques guided by age-matched infant atlases. While surface-based registration approaches have become increasingly popular in studies involving older populations (Glasser et al., 2016), its application to early brain development has been limited due to the challenges involved in the construction of accurate cortical surfaces and age-appropriate atlases.

Our analysis on a cohort of 289 term-born neonates (age at scan: 37.4 - 44.8 weeks) shows that the surface-based Bayesian approach can produce clean estimates of subject-level cortical RSNs using only 10 minutes of individual fMRI data. The statistical framework enables the computation of subject-level t-statistic maps which, in turn, allows for improved estimation of functional parcellations at the subject-level. As a result, we observed individual topological differences hidden by group-level averages. Furthermore, a positive relationship between age and subject-level connectivity strength was revealed for almost all cortical RSNs, confirming the hypothesis that the functional connectome matures with age in healthy term-born infants. Importantly, our work extends beyond existing research by showing that significant maturational changes are not only restricted to primary sensory networks but also present in higher-order networks in the first weeks of postnatal life. These results illustrate the potential advantages of combining surface-based processing and template-based approaches to inform individual variability in very young populations, opening the door to precision neuroimaging studies of early brain development with enhanced accuracy and reliability.

Methods

Subjects and data acquisition

MRI data was obtained from the second release of the dHCP database. For this study, we only considered term-born infants (i.e. postmenstrual age (PMA) > 36 weeks) with radiological score lesser than three, indicating lesions of no clinical or analytical significance (see dHCP release notes for details). Following these criteria, 289 term-born infants (age at birth: 37.1 – 42.3 weeks PMA) scanned shortly after birth (age at scan: 37.4 – 44.8 weeks PMA) were considered for further analysis.

All scans were obtained with a 3T Philips Achieva using a dedicated neonatal head-coil at the Evelina Newborn Imaging Center. Both T1-weighted (TR = 4795 ms; TE = 8.7 ms) and T2-weighted (TR = 12 s; TE = 156 ms) structural scans were obtained with a multi-slice Turbo Spin Echo (TSE) sequence, with in-plane resolution 0.8 x 0.8 mm^2 and 1.6 mm slices overlapped by 0.8 mm. Two stacks of images were taken per weighting, sagittal and axial, which were integrated to obtain T2w volumes with an image resolution of 0.8 mm isotropic. Blood oxygen level-dependent (BOLD) scans were obtained with a multi-slice gradient-echo echo planar imaging (EPI) sequence (TE = 38 ms; TR = 392 ms, multiband factor = 9; flip angle = 34°) with an image resolution of 2.15 mm isotropic. A resting-state BOLD fMRI acquisition of 2300 time points (15 minutes) was obtained for each infant.

MRI preprocessing

Cortical surfaces

After brain extraction using a modified version of FSL BET for unmyelinated brains, tissue specific masks corresponding to gray matter, low, and high intensity white matter were segmented from the brain-extracted T2w images using the Draw-EM tool (Makropoulos et al., 2014). Individual surfaces corresponding to white matter, pial and midthickness were created using these tissue masks as described in Makropoulos et al., 2018.

For the rest of the analysis, a 40-week symmetrical atlas consisting of 55,400 cortical vertices built from the dHCP cohort (Williams et al., 2021) was used. The original atlas in Bozek et al., 2018 was built based on a spherical registration approach using the Multimodal Surface Matching (MSM) tool for aligning cortical folding (Robinson et al., 2018). For this extended version, left-right vertex correspondence was enforced by co-registering right and left sulcal depth maps during alignment.

We used the MSM approach to register each individual cortical surface to the symmetrical 40-week atlas, concatenating single-week transformations to avoid the accumulation of approximation errors. The spherical registrations from this process were later used when mapping the BOLD fMRI data onto the atlas surface.

Functional data

Resting-state BOLD fMRI data were preprocessed using a modified version of the Human Connectome Project (HCP) (Glasser et al., 2013) pipeline specifically developed for the dHCP (Fitzgibbon et al., 2020). Preprocessing steps were performed on the BOLD volumes in native space and included: (1) field map correction, (2) intra- and inter-volume motion correction, (3) high-pass filtering to remove slow drifts, and (4) spatial ICA using FSL FIX (Griffanti et al., 2014; Salimi-Khorshidi et al., 2014) to regress out structured noise artifacts.

To further reduce the potential effect of motion on functional connectivity measures, we adopted a conservative frame censoring approach. Emerging evidence suggests that head motion is correlated with neurophysiological states (e.g., sleep state) (Denisova, 2019). Since aggressive frame censoring may introduce heterogeneities in the BOLD time series associated with different physiological states, we retained a contiguous block of data to minimize this potential issue. Following the criteria proposed in Eyre et al., 2021, frames with DVARS (root mean-squared BOLD signal intensity change) higher than 1.5 times the interquartile range above the 75th percentile within a session were considered corrupted by motion. A contiguous block of 1600 frames with the minimum number of motion outliers was retained for each session. Any session with more than 160 motion-corrupted frames (10%) within the contiguous block was excluded from further analysis.

The volumetric resting-state BOLD data was mapped onto the individual cortical surfaces using the HCP surface pipeline (Glasser et al., 2013) as implemented in Connectome Workbench. The surface-based BOLD data was then mapped onto the custom 40-week atlas surface using spherical registration (as described in §*Cortical surfaces*). Finally, the individual datasets were spatially smoothed using a geodesic 2D Gaussian kernel (FWHM = 3 mm).

Temporal signal-to-noise ratio

We computed a measure of temporal signal-to-noise ratio (tSNR) as the ratio between the mean BOLD signal and its standard deviation. A global tSNR map was built in decibels [dB] by averaging the individual tSNR maps across the whole sample as

$$tSNR(v)[dB] = 10\log_{10}\frac{\sum_{i=1}^{N} SNR_i(v)}{N} \tag{1}$$

where, for each subjcet i, the SNR is calculated for each vertex v.

As expected from the patterns associated with susceptibility artifacts in BOLD data and previous similar analysis (Fitzgibbon et al., 2020; Thomas Yeo et al., 2011), we observe areas of particularly low tSNR in the inferior and medial temporal lobe, orbitofrontal and insular cortices (Fig. S3).

Bayesian subject-level ICA

To estimate subject-level RSNs, we use a custom implementation of template ICA (Mejia et al., 2020), an extension of probabilistic ICA (C. Beckmann and Smith, 2004). In this section, we describe the template-based ICA model, the calculation of empirical population priors, and the strategy for estimating individual posterior mean and variance.

Template-based ICA model

For each subject i, the dimensionally reduced BOLD fMRI data $\mathbf{y}_i$ with T time-points is modeled at vertex v as

$$\mathbf{y}_i(v) = \mathbf{A}_i\mathbf{s}_i(v) + \mathbf{e}_i(v), \quad \mathbf{e}_i(v) \sim N(0, \Omega) \tag{2}$$

where $\mathbf{A}_i^{(T\times Q)}$ is the mixing matrix, $\mathbf{s}_i^{(Q\times 1)}$ represents the Q independent components (ICs) associated with a different RSN, and $\mathbf{e}_i^{(T\times 1)}$ represents any source of Gaussian noise with variance Ω. Like in probabilistic ICA, $\mathbf{y}_i$ is obtained using single value decomposition (SVD) of the preprocessed BOLD dataset, and an estimate of the Gaussian noise variance $\mathbf{\Omega}$ is obtained as the residual variance. Note that the error in equation 2 has a Gaussian distribution since we assume that any source of non-Gaussian noise is eliminated after ICA-FIX on each preprocessed BOLD dataset.

In the template ICA model, we further characterize each IC as

$$\mathbf{s}_i(v) = \mu_0(v) + \delta_i(v), \quad \delta_i(v) \sim N(0, \mathbf{\Sigma_0}(v)) \tag{3}$$

where $\mu_0(v)^{(Q\times 1)}$ is the group-level mean, and $\delta_i(v)^{(Q\times 1)}$ represents subject-level deviations denoting unique features of spatial topology associated to each RSN. We assume that the $\delta_i(v)$ are normally distributed with covariance matrix $\mathbf{\Sigma}_v = diag\{\nu_1^2(v), \nu_2^2(v), ..., \nu_q^2(v)\}$ where each ${\sigma_{0q}}^2$ is the between-subject variance associated to each IC q at each vertex v.

For a subject-specific BOLD dataset $\mathbf{y}_i(v)$, the proposed problem can be formulated within a Bayesian framework where we aim to obtain a vertex-wise posterior distribution for the subject-level IC maps $\mathbf{s}_i(v)$, given a set of population

priors or templates (mean $\mu_0(v)$ and between-subject variance $\mathbf{\Sigma}_0(v)$). Note that the vertex-wise posterior spatial maps $\mathbf{s}_i$ are assumed to be normally distributed with a subject-level mean μ_i and variance σ_i.

To estimate the posterior mean and variance of the subject-level ICs, along with the model parameters including the mixing matrix and residual variance, a computationally efficient expectation-maximization (EM) algorithm was utilized (see §*Estimation of individual posterior mean and variance*) and Figure 1 for a description of the estimation procedure).

Empirical population priors

The Bayesian framework relies on empirical population priors, which consist of estimates of the mean and between-subject variance of a set of ICs. To first define the set of ICs, we performed group ICA (C. F. Beckmann et al., 2005) on a subset of 24 subjects (scanned between 43.5 and 45 weeks PMA) using FSL MELODIC (C. Beckmann and Smith, 2004). The number of ICs was set at 20 to achieve a balance between robustness and similarity to previous analysis on infants (Doria et al., 2010; Eyre et al., 2021; Rajasilta et al., 2020; Toulmin et al., 2015). Fourteen ICs were associated to relevant cortical networks or subnetworks, namely, medial motor, lateral motor, auditory, somatosensory, primary visual, motor association, prefrontal, language, visual association (left and right), posterior cingulate cortex, frontoparietal, posterior parietal, and inferior parietal (Fig. 4). To obtain rough point estimates of individual IC maps and then obtain population mean and between-subject variance estimates, dual regression (Nickerson et al., 2017) was applied to a subset of subjects (N = 35) uniformly scanned between 37 and 43 weeks PMA. To calculate the between-subject variability, each individual BOLD time series was divided into two halves (or pseudo-sessions) prior to dual regression. The population mean $\mu_0(v)$ for each IC q was estimated as

$$\mu_{0_q}(v) = \frac{1}{2N}\sum_{i=1}^{N}\sum_{j=1}^{2} s_{ij}(q,v) \tag{4}$$

where $s_{ij}(q,v)$ is the dual regression IC estimate for each subject i and each session j.

The between-subject variance is obtained by decomposing the total variance into within- and between-subject components. The total variance for each individual IC at each vertex was estimated as the average of the variance obtained for each pseudo-session,

$$\sigma^2_{tot,q}(v) = \frac{1}{2}\sum_{j=1}^{2} \mathrm{Var}_i\{s_{ij}(q,v)\} \tag{5}$$

while the within-subject variance was estimated as the variance of the difference between the individual ICs estimated from each pseudo-session

$$\sigma^2_{noise,q}(v) = \frac{1}{2}\mathrm{Var}_i\{s_{i2}(q,v) - s_{i1}(q,v)\} \tag{6}$$

Finally, from equations 5 and 6, the between-subject variance was estimated as the difference between the total and within-subject variances

$$\sigma^2_{0_q}(v) = \sigma^2_{tot,q}(v) - \sigma^2_{noise,q}(v) \tag{7}$$

where the σ_{0_q} are the diagonal elements of the covariance matrix $\mathbf{\Sigma}_0$ in equation 2, representing the variance of the empirical population prior.

Estimation of individual posterior mean and variance

A schematic of the estimation procedure is shown in Figure 1. The EM algorithm requires an initial estimate of the parameters Ω and $\mathbf{A_i}$. $\mathbf{A_i^{(0)}}$ was obtained from the dual regression procedure described above. Gaussian noise variance $\sigma_0^{(0)}$ was estimated from the residual variance of the dimensionality reduction of the BOLD data.

These two parameters were updated at every iteration of the EM algorithm by maximizing the expected log-likelihood. Alternately, conditional on the current estimate of the parameters, the posterior distribution of the subject-level ICs $\mathbf{s_i}$ was updated to obtain the posterior moments required for the parameter maximum likelihood estimations. The algorithm was run until convergence of the parameter estimators, and the posterior mean $\hat{\mu}_\mathbf{i}$ and variance $\hat{\sigma}_\mathbf{i}$ of $\hat{s}_i(v, y, \theta)$ were obtained. A representation of the entire pipeline is shown in Figure S1.

Results

Individual patterns of functional connectivity

Using only 10 minutes of resting-state fMRI data, we identified 14 cortical RSNs (represented by independent components, ICs) in individual subjects from a cohort of 254 full-term infants (note that the 35 subjects considered in the estimation of the empirical population priors were excluded from further analysis). Overall, the surface-based Bayesian approach produced cleaner estimates of subject-level IC maps than dual regression, as illustrated by five representative IC maps obtained in a single infant (Fig. 2). Notably, the Bayesian approach removed clusters of spurious activations present in the dual regression maps (see for example the insular cortex in the medial motor IC maps of Figure 2) . Other improvements include the emergence of more defined clusters in distributed networks, as shown in the frontal cluster of the language IC maps. A complete set of subject-level IC maps obtained for both methods is included in Figure S2.

To perform comparisons across subjects, we computed t-statistic maps from the subject-specific posterior mean and standard error maps estimated by the surface-based Bayesian model. Figure 3 shows the unthresholded t-statistic maps for five networks and three term-born infants scanned at different postmenstrual ages within a period of four weeks. While a general spatial topology is preserved for each specific network, individual differences are evident across subjects. For example, the temporal cluster of the inferior parietal IC map of subject C seems more defined than in

subjects A and B. Similarly, the frontal cluster of the language IC map of subject A shows a stronger "activation" in comparison with subjects B and C.

As an alternative way to summarize the individual differences observed in Figure 3, we used a winner-takes-all strategy to compute subject-level functional parcellations (Fig. 4) in which a network label was assigned to each vertex based on the highest t-score at that location. The Bayesian approach constitutes a compromise between robust group-level RSNs provided by the population template and subject-level RSNs associated to the individual data. This can be better appreciated by looking at the functional parcellation maps obtained for the group ICA maps and the subject-level parcellations for three different infants (Fig. 4). Even though a general resemblance to the group-level parcellation is preserved, remarkable individual differences in shape, size, and location of the individual parcels are evident across subjects (see for example the significantly reduced frontal cluster of the language IC map in the left hemisphere of Subject A , while present for the in comparison with the other individuals).

Effect of age at scan

To explore whether the observed differences could be partially explained by maturational factors, we estimated the Spearman's rank correlation coefficient between age at scan and individual connectivity strength for each network, after controlling for sex and motion. Individual connectivity strength was defined as the mean t-score within the areas of significant engagement for each subject-level IC. Areas of significant engagement were estimated from a t-test on each pair of posterior mean and standard error IC maps, after Bonferroni correction for multiple comparisons. Within-network connectivity significantly increased with age at scan (37.4 – 44.8 weeks) for almost all cortical ICs, including medial motor, lateral motor, somatosensory, auditory, visual, motor association, inferior parietal, posterior parietal, frontoparietal, language, visual association left, and visual association right networks (Fig. 5). The only ICs not showing significant associations with age were those corresponding to the prefrontal and posterior cingulate cortex networks. Statistical significance was defined as monotonic trends with a p-value lower than 0.05, as calculated using the AS 89 algorithm implemented in the 'stats' R-package.

Inter-subject variability

To quantify the spatial variability across individuals, we estimated a frequency map from the subject-level parcellations. Figure 6 shows the percentage of subjects that share the same label or parcel at each cortical vertex. Given that multiple labels may contribute to the same vertex in different subjects, the frequency map only shows the percentage of subjects associated to the dominant label at each location. In addition to all primary networks, the visual association, language, and parietal networks appear clearly defined in the frequency map and exhibit a high spatial overlap. In contrast, the clusters associated with the inferior parietal, frontoparietal, and prefrontal networks exhibit lower spatial overlap across individuals.

Discussion

The existence of resting-state networks (RSNs) is well documented in adults. In neonates, several studies have demonstrated the presence of recognizable, albeit sometimes incomplete, RSNs at the group level (Doria et al., 2010; Eyre et al., 2021; Gao et al., 2015; Smyser et al., 2010). This study extends beyond existing research by characterizing RSNs in term-born neonates at the subject-level, leveraging several technical improvements to elucidate individual differences and developmental trajectories within the first weeks of life. To achieve these results, we utilized surface-based methods and age-matched atlases to mitigate co-registration errors and partial volume effects. In addition, we propose a Bayesian approach that offers a powerful statistical framework to obtain clean estimates of subject-level RSNs using a limited amount of individual data.

Using these methodological innovations, we were able to identify topological differences across subjects hidden by group-level results. This is in line with studies done in adults that show that areas of common activation obscure individual connectivity features (Gordon et al., 2017; Hermosillo et al., 2022; Michon et al., 2022). Indeed, inter-subject differences are evident across the individual t-maps (Fig. 3) and functional parcellations (Fig. 4) obtained for different infants. Interestingly, the individual parcellations also show topological differences with respect to the group-level parcellation (note, for example, that the temporal cluster of the frontoparietal network is present in the individual parcellations but absent in the group-level parcellation possibly due to its variable location across subjects). It is notable that despite these differences, the results show adult-like higher-order RSNs maps already present at birth – albeit sometimes in sparser, precursory form (Fig. 3).

To quantitatively assess these individual differences, we studied the relationship between subject-level RSNs and age at scan. As in previous reports, significant maturation is observed in all primary sensory RSNs, as measured by the correlation between network strength and age at scan (Fig. 5) (Doria et al., 2010; Eyre et al., 2021; Gao et al., 2015; Hu et al., 2022; Smyser et al., 2010). Furthermore, contrary to prior studies, we note a clear developmental trajectory within a five-week window for most of the independent components (ICs) linked to higher-order RSNs, except for the prefrontal and posterior cingulate cortices.

The frequency maps depicting the spatial overlap of networks across subjects reveal a pattern that progresses from posterior to anterior regions (Fig. 6). In particular, we observe high levels of spatial overlap in the primary sensory networks, along with the higher-order networks located in the posterior regions. In contrast, the prefrontal network displays low spatial overlap which can be attributed to developmental factors, as supported by histological findings (Keunen et al., 2017). Notably, there are other regions characterized by low spatial overlap, namely, the boundaries between the different RSNs as well as the insular and inferior temporal cortices. The lack of consistency in the delineation of boundaries between the RSNs reflects the topological variability that our study aims to capture. However, the limited overlap observed in the insula and inferior temporal cortices may be associated with elevated levels of noise in the BOLD signals, as demonstrated by the SNR map obtained for this specific cohort (Fig. S3).

Subject-level inference produces more accurate descriptions of brain organization

We hypothesize that variability in the spatial distribution of RSNs across individuals could be the primary factor that hinders the identification of population-level trends and renders growth curves challenging to obtain, especially for distributed higher-order RSNs. In contrast to prior studies, the use of individual regions of interest (ROIs) enabled us to achieve improved outcomes in terms of estimating connectivity strength at the individual level. This is consistent with previous reports showing group-average ROIs that lead to inflated or under-estimated group differences (Levi et al., 2023).

The trend towards individual inference instead of group analysis has emerged as a recent focus in precision neuroimaging. This approach not only facilitates the acquisition of relevant individual insights in the clinic but also plays a critical role in aggregating individual data without diluting individual features (Gordon et al., 2017; Laumann et al., 2015; Michon et al., 2022). To achieve acceptable levels of reliability at the individual level, extensive amounts of imaging data need to be collected, which is rarely practical in infants who are typically scanned during natural sleep. As an alternative, we propose an empirical Bayesian model (Mejia et al., 2020) that leverages the growing volume of neonatal data available in existing databases such as the dHCP database. The proposed model produces more accurate subject-level RSNs maps by shrinking to the empirical population prior in subject-specific areas of low SNR while maintaining the individual differences.

More advanced techniques are crucial to maintain precision mapping

Concurrently, we used additional technical enhancements to mitigate any biases that could potentially skew our results towards adult populations. To eliminate any distortions that may arise from mapping neonatal brains onto an adult-based atlas, we utilized a symmetrical atlas (Bozek et al., 2018; Williams et al., 2021) derived from the dHCP cohort. This atlas served as a reference surface onto which the individual BOLD timeseries were projected. To prevent the accumulation of approximation errors, the transformation from the individual to the reference surface was computed as concatenated week-to-week transformations.

Moreover, the adoption of surface-based analysis effectively reduces the potential influence of partial volume effects encountered in volumetric analysis. This is particularly evident when applying spatial smoothing to BOLD signals. By working on cortical surfaces, contamination between functional regions on opposite sides of a sulcus is effectively avoided (Brodoehl et al., 2020). This is because 2D geodesic distances, which are more neurobiologically relevant, are employed instead of 3D volumetric distances (Glasser et al., 2013).

Methodological considerations

The selection of the number of independent components in the group ICA was based on previous work with this cohort (Eyre et al., 2021; Molloy and Saygin, 2022; Nielsen et al., 2022) as well as adult parcellations (Gordon et al., 2016; Yeo et al., 2011). While this collection of studies includes both hard and soft parcellations ranging from 7 to 30 components,

the exact number that strikes a balance between functional homogeneity and interpretability remains an open debate (Gordon et al., 2016). For consistency with the latest studies on this dataset, where 30 components were used to describe volumetric RSNs (Eyre et al., 2021), we opted for 20 components for our surface-based analysis that excludes any subcortical regions. Subsequently, we find that both group ICA and the individual parcellations align with biologically relevant areas previously associated with increased neuronal activity in adult task-based experiments (Nickerson, 2018; Smith et al., 2009).

Head movement modulated by arousal states may influence the resting-state functional connectivity patterns in infants (Mitra et al., 2017). Indeed, it is plausible that certain infants may exhibit increased alertness or be in a state of active sleep, leading to increased head movement compared to other infants who are in a quiet sleep state (Denisova, 2019). Applying an aggressive frame censoring approach that selectively retains BOLD data segments with minimal motion can introduce a potential systematic bias towards subjects or data segments associated with a particular state. Thus, to mitigate any potential bias influenced by the arousal state of the infants, we implemented a conservative frame censoring approach. This approach guarantees an equal number of consecutive frames for each subject, ensuring that the segments remained qualitatively and quantitatively comparable across the entire cohort.

Conclusions

Leveraging shared information across subjects produced cleaner estimates of individual functional connectivity maps in neonates than classic RSFC analyses. Improved detection of individual differences was evidenced by a maturational path in almost all brain regions. Importantly, our work extends beyond existing research by showing that significant maturational changes are not only restricted to primary sensory networks but also present in higher-association networks in the first weeks of postnatal life. These results illustrate the potential advantages of combining surface-based processing and template-based approaches to inform individual variability in very young populations, opening the door to precision neuroimaging studies of early brain development with enhanced accuracy and reliability.

Data and code availability

The neonatal data in this study is part of the second release of the developing Human Connectome Project and are available to download (https://www.developingconnectome.org). The cortical atlas is also publicly available (https://brain-development.org/brain-atlases/atlases-from-the-dhcp-project/cortical-surface-atlas-bozek/). The in-house code used in this study includes shell scripts, python scripts, and R impelemantions of the templateICAr (https://github.com/mandymejia/templateICAr) and ciftiTools (Pham et al., 2022) libraries. A version of the code, edited for clarity, will be available and maintained on https://github.com/diegoderman/babybayes.

Acknowledgments

Data were provided by the developing Human Connectome Project, KCL-Imperial-Oxford Consortium funded by the European Research Council under the European Union Seventh Framework Programme (FP/2007-2013) / ERC Grant Agreement no. [319456]. We are grateful to the families who generously supported this work. The non-dHCP pipeline analyses were performed on the Indiana University HPC Cluster (https://uits.iu.edu/).

References

Beckmann, C., & Smith, S. (2004). Probabilistic Independent Component Analysis for Functional Magnetic Resonance Imaging. *IEEE Transactions on Medical Imaging*, *23*(2), 137–152. https://doi.org/10.1109/TMI.2003.822821

Beckmann, C. F., DeLuca, M., Devlin, J. T., & Smith, S. M. (2005). Investigations into resting-state connectivity using independent component analysis. *Philosophical Transactions of the Royal Society B: Biological Sciences*, *360*(1457), 1001–1013. https://doi.org/10.1098/rstb.2005.1634

Birn, R. M., Molloy, E. K., Patriat, R., Parker, T., Meier, T. B., Kirk, G. R., Nair, V. A., Meyerand, M. E., & Prabhakaran, V. (2013). The effect of scan length on the reliability of resting-state fMRI connectivity estimates. *NeuroImage*, *83*, 550–558. https://doi.org/10.1016/j.neuroimage.2013.05.099

Bozek, J., Makropoulos, A., Schuh, A., Fitzgibbon, S., Wright, R., Glasser, M. F., Coalson, T. S., O'Muircheartaigh, J., Hutter, J., Price, A. N., Cordero-Grande, L., Teixeira, R. P. A., Hughes, E., Tusor, N., Baruteau, K. P., Rutherford, M. A., Edwards, A. D., Hajnal, J. V., Smith, S. M., . . . Robinson, E. C. (2018). Construction of a neonatal cortical surface atlas using multimodal surface matching in the developing human connectome project. *NeuroImage*, *179*, 11–29. https://doi.org/10.1016/j.neuroimage.2018.06.018

Brodoehl, S., Gaser, C., Dahnke, R., Witte, O. W., & Klingner, C. M. (2020). Surface-based analysis increases the specificity of cortical activation patterns and connectivity results [Number: 1]. *Scientific Reports*, *10*(1), 5737. https://doi.org/10.1038/s41598-020-62832-z

Cao, M., Shu, N., Cao, Q., Wang, Y., & He, Y. (2014). Imaging functional and structural brain connectomics in attention-deficit/hyperactivity disorder. *Molecular Neurobiology*, *50*(3), 1111–1123. https://doi.org/10.1007/s12035-014-8685-x

Denisova, K. (2019). Neurobiology, not artifacts: Challenges and guidelines for imaging the high risk infant. *NeuroImage*, *185*, 624–640. https://doi.org/10.1016/j.neuroimage.2018.07.023

DeSocio, J. E. (2018). Epigenetics, maternal prenatal psychosocial stress, and infant mental health. *Archives of Psychiatric Nursing*, *32*(6), 901–906. https://doi.org/10.1016/j.apnu.2018.09.001

Doria, V., Beckmann, C. F., Arichi, T., Merchant, N., Groppo, M., Turkheimer, F. E., Counsell, S. J., Murgasova, M., Aljabar, P., Nunes, R. G., Larkman, D. J., Rees, G., & Edwards, A. D. (2010). Emergence of resting state networks in the preterm human brain. *Proceedings of the National Academy of Sciences*, *107*(46), 20015–20020. https://doi.org/10.1073/pnas.1007921107

Edwards, A. D., Rueckert, D., Smith, S. M., Abo Seada, S., Alansary, A., Almalbis, J., Allsop, J., Andersson, J., Arichi, T., Arulkumaran, S., Bastiani, M., Batalle, D., Baxter, L., Bozek, J., Braithwaite, E., Brandon, J., Carney, O., Chew, A., Christiaens, D., … Hajnal, J. V. (2022). The Developing Human Connectome Project Neonatal Data Release. *Frontiers in Neuroscience*, *16*, 886772. https://doi.org/10.3389/fnins.2022.886772

Eyre, M., Fitzgibbon, S. P., Ciarrusta, J., Cordero-Grande, L., Price, A. N., Poppe, T., Schuh, A., Hughes, E., O'Keeffe, C., Brandon, J., Cromb, D., Vecchiato, K., Andersson, J., Duff, E. P., Counsell, S. J., Smith, S. M., Rueckert, D., Hajnal, J. V., Arichi, T., … Edwards, A. D. (2021). The developing human connectome project: Typical and disrupted perinatal functional connectivity [Number: 7]. *Brain*, *144*(7), 2199–2213. https://doi.org/10.1093/brain/awab118

Fitzgibbon, S. P., Harrison, S. J., Jenkinson, M., Baxter, L., Robinson, E. C., Bastiani, M., Bozek, J., Karolis, V., Cordero Grande, L., Price, A. N., Hughes, E., Makropoulos, A., Passerat-Palmbach, J., Schuh, A., Gao, J., Farahibozorg, S.-R., O'Muircheartaigh, J., Ciarrusta, J., O'Keeffe, C., … Andersson, J. (2020). The developing Human Connectome Project (dHCP) automated resting-state functional processing framework for newborn infants. *NeuroImage*, *223*, 117303. https://doi.org/10.1016/j.neuroimage.2020.117303

Gao, W., Alcauter, S., Smith, J. K., Gilmore, J. H., & Lin, W. (2015). Development of human brain cortical network architecture during infancy. *Brain Structure and Function*, *220*(2), 1173–1186. https://doi.org/10.1007/s00429-014-0710-3

Glasser, M. F., Smith, S. M., Marcus, D. S., Andersson, J. L. R., Auerbach, E. J., Behrens, T. E. J., Coalson, T. S., Harms, M. P., Jenkinson, M., Moeller, S., Robinson, E. C., Sotiropoulos, S. N., Xu, J., Yacoub, E., Ugurbil, K., & Van Essen, D. C. (2016). The Human Connectome Project's neuroimaging approach [Excelente justificación de surface-based analysis.

WARNING: Este paper tiene un montón de material suplementario, con la mayoría de las imágenes.]. *Nature Neuroscience*, *19*(9), 1175–1187. https://doi.org/10.1038/nn.4361

Glasser, M. F., Sotiropoulos, S. N., Wilson, J. A., Coalson, T. S., Fischl, B., Andersson, J. L., Xu, J., Jbabdi, S., Webster, M., Polimeni, J. R., Van Essen, D. C., & Jenkinson, M. (2013). The minimal preprocessing pipelines for the human connectome project. *NeuroImage*, *80*, 105–124. https://doi.org/10.1016/j.neuroimage.2013.04.127

Gordon, E. M., Laumann, T. O., Adeyemo, B., Huckins, J. F., Kelley, W. M., & Petersen, S. E. (2016). Generation and evaluation of a cortical area parcellation from resting-state correlations [Number: 1]. *Cerebral Cortex*, *26*(1), 288–303. https://doi.org/10.1093/cercor/bhu239

Gordon, E. M., Laumann, T. O., Gilmore, A. W., Newbold, D. J., Greene, D. J., Berg, J. J., Ortega, M., Hoyt-Drazen, C., Gratton, C., Sun, H., Hampton, J. M., Coalson, R. S., Nguyen, A. L., McDermott, K. B., Shimony, J. S., Snyder, A. Z., Schlaggar, B. L., Petersen, S. E., Nelson, S. M., & Dosenbach, N. U. (2017). Precision functional mapping of individual human brains. *Neuron*, *95*(4), 791–807.e7. https://doi.org/10.1016/j.neuron.2017.07.011

Griffanti, L., Salimi-Khorshidi, G., Beckmann, C. F., Auerbach, E. J., Douaud, G., Sexton, C. E., Zsoldos, E., Ebmeier, K. P., Filippini, N., Mackay, C. E., Moeller, S., Xu, J., Yacoub, E., Baselli, G., Ugurbil, K., Miller, K. L., &

Smith, S. M. (2014). ICA-based artefact removal and accelerated fMRI acquisition for improved resting state network imaging. *NeuroImage*, *95*, 232–247. https://doi.org/10.1016/j.neuroimage.2014.03.034

He, L., Li, H., Holland, S. K., Yuan, W., Altaye, M., & Parikh, N. A. (2018). Early prediction of cognitive deficits in very preterm infants using functional connectome data in an artificial neural network framework. *NeuroImage: Clinical*, *18*, 290–297. https://doi.org/10.1016/j.nicl.2018.01.032

Hermosillo, R. J., Moore, L. A., Fezcko, E., Dworetsky, A., Pines, A., Conan, G., Mooney, M. A., Randolph, A., Adeyemo, B., Earl, E., Perrone, A., Carrasco, C. M., Uriarte-Lopez, J., Snider, K., Doyle, O., Cordova, M., Nagel, B. J., Feldstein Ewing, S. W., Satterthwaite, T., … Fair, D. A. (2022, January 13). *A precision functional atlas of network probabilities and individual-specific network topography* (preprint). Neuroscience. https://doi.org/10.1101/2022.01.12.475422

Hu, D., Wang, F., Zhang, H., Wu, Z., Zhou, Z., Li, G., Wang, L., Lin, W., Li, G., & UNC/UMN Baby Connectome Project Consortium. (2022). Existence of functional connectome fingerprint during infancy and its stability over months [Number: 3]. *The Journal of Neuroscience*, *42*(3), 377–389. https://doi.org/10.1523/JNEUROSCI.0480-21.2021

Keunen, K., Counsell, S. J., & Benders, M. J. (2017). The emergence of functional architecture during early brain development. *NeuroImage*, *160*, 2–14. https://doi.org/10.1016/j.neuroimage.2017.01.047

Laumann, T. O., Gordon, E. M., Adeyemo, B., Snyder, A. Z., Joo, S. J., Chen, M.-Y., Gilmore, A. W., McDermott, K. B., Nelson, S. M., Dosenbach, N. U., Schlaggar, B. L., Mumford, J. A., Poldrack, R. A., & Petersen, S. E. (2015). Functional System and Areal Organization of a Highly Sampled Individual Human Brain. *Neuron*, *87*(3), 657–670. https://doi.org/10.1016/j.neuron.2015.06.037

Levi, P. T., Chopra, S., Pang, J. C., Holmes, A., Sassenberg, T. A., DeYoung, C. G., & Fornito, A. (2023, January 5). *The effect of using group-averaged or individualized brain parcellations when investigating connectome dysfunction: A case study in psychosis* (preprint). Psychiatry and Clinical Psychology. https://doi.org/10.1101/2023.01.03.23284124

Makropoulos, A., Gousias, I. S., Ledig, C., Aljabar, P., Serag, A., Hajnal, J. V., Edwards, A. D., Counsell, S. J., & Rueckert, D. (2014). Automatic Whole Brain MRI Segmentation of the Developing Neonatal Brain. *IEEE Transactions on Medical Imaging*, *33*(9), 1818–1831. https://doi.org/10.1109/TMI.2014.2322280

Makropoulos, A., Robinson, E. C., Schuh, A., Wright, R., Fitzgibbon, S., Bozek, J., Counsell, S. J., Steinweg, J., Vecchiato, K., Passerat-Palmbach, J., Lenz, G., Mortari, F., Tenev, T., Duff, E. P., Bastiani, M., Cordero-Grande, L., Hughes, E., Tusor, N., Tournier, J.-D., … Rueckert, D. (2018). The developing human connectome project: A minimal processing pipeline for neonatal cortical surface reconstruction. *NeuroImage*, *173*, 88–112. https://doi.org/10.1016/j.neuroimage.2018.01.054

Mejia, A. F., Nebel, M. B., Wang, Y., Caffo, B. S., & Guo, Y. (2020). Template independent component analysis: Targeted and reliable estimation of subject-level brain networks using big data population priors [Number: 531]. *Journal of the American Statistical Association*, *115*(531), 1151–1177. https://doi.org/10.1080/01621459.2019.1679638

Merhar, S. L., Jiang, W., Parikh, N. A., Yin, W., Zhou, Z., Tkach, J. A., Wang, L., Kline-Fath, B. M., He, L., Braimah, A., Vannest, J., & Lin, W. (2021). Effects of prenatal opioid exposure on functional networks in infancy. *Developmental Cognitive Neuroscience*, *51*, 100996. https://doi.org/10.1016/j.dcn.2021.100996

Michon, K. J., Khammash, D., Simmonite, M., Hamlin, A. M., & Polk, T. A. (2022). Person-specific and precision neuroimaging: Current methods and future directions. *NeuroImage*, *263*, 119589. https://doi.org/10.1016/j.neuroimage.2022.119589

Mitra, A., Snyder, A. Z., Tagliazucchi, E., Laufs, H., Elison, J., Emerson, R. W., Shen, M. D., Wolff, J. J., Botteron, K. N., Dager, S., Estes, A. M., Evans, A., Gerig, G., Hazlett, H. C., Paterson, S. J., Schultz, R. T., Styner, M. A., Zwaigenbaum, L., The IBIS Network, … Raichle, M. (2017). Resting-state fMRI in sleeping infants more closely resembles adult sleep than adult wakefulness (S. Hayasaka, Ed.). *PLOS ONE*, *12*(11), e0188122. https://doi.org/10.1371/journal.pone.0188122

Molloy, M. F., & Saygin, Z. M. (2022). Individual variability in functional organization of the neonatal brain. *NeuroImage*, *253*, 119101. https://doi.org/10.1016/j.neuroimage.2022.119101

Nickerson, L. D. (2018). Replication of resting state-task network correspondence and novel findings on brain network activation during task fMRI in the human connectome project study [Number: 1]. *Scientific Reports*, *8*(1), 17543. https://doi.org/10.1038/s41598-018-35209-6

Nickerson, L. D., Smith, S. M., Öngür, D., & Beckmann, C. F. (2017). Using dual regression to investigate network shape and amplitude in functional connectivity analyses. *Frontiers in Neuroscience*, *11*. https://doi.org/10.3389/fnins.2017.00115

Nielsen, A. N., Kaplan, S., Meyer, D., Alexopoulos, D., Kenley, J. K., Smyser, T. A., Wakschlag, L. S., Norton, E. S., Raghuraman, N., Warner, B. B., Shimony, J. S., Luby, J. L., Neil, J. J., Petersen, S. E., Barch, D. M., Rogers, C. E., Sylvester, C. M., & Smyser, C. D. (2022). Maturation of large-scale brain systems over the first month of life. *Cerebral Cortex*, bhac242. https://doi.org/10.1093/cercor/bhac242

Pham, D. D., Muschelli, J., & Mejia, A. F. (2022). ciftiTools: A package for reading, writing, visualizing, and manipulating CIFTI files in r. *NeuroImage*, *250*, 118877. https://doi.org/10.1016/j.neuroimage.2022.118877

Rajasilta, O., Tuulari, J. J., Björnsdotter, M., Scheinin, N. M., Lehtola, S. J., Saunavaara, J., Häkkinen, S., Merisaari, H., Parkkola, R., Lähdesmäki, T., Karlsson, L., & Karlsson, H. (2020). Resting-state networks of the neonate brain identified using independent component analysis. *Developmental Neurobiology*, *80*(3-4), 111–125. https://doi.org/10.1002/dneu.22742

Robinson, E. C., Garcia, K., Glasser, M. F., Chen, Z., Coalson, T. S., Makropoulos, A., Bozek, J., Wright, R., Schuh, A., Webster, M., Hutter, J., Price, A., Cordero Grande, L., Hughes, E., Tusor, N., Bayly, P. V., Van Essen, D. C., Smith, S. M., Edwards, A. D., … Rueckert, D. (2018). Multimodal surface matching with higher-order smoothness constraints. *NeuroImage*, *167*, 453–465. https://doi.org/10.1016/j.neuroimage.2017.10.037

Salimi-Khorshidi, G., Douaud, G., Beckmann, C. F., Glasser, M. F., Griffanti, L., & Smith, S. M. (2014). Automatic denoising of functional MRI data: Combining independent component analysis and hierarchical fusion of classifiers. *NeuroImage*, *90*, 449–468. https://doi.org/10.1016/j.neuroimage.2013.11.046

Sandman, C. A., Davis, E. P., Buss, C., & Glynn, L. M. (2012). Exposure to prenatal psychobiological stress exerts programming influences on the mother and her fetus. *Neuroendocrinology*, *95*(1), 8–21. https://doi.org/10.1159/000327017

Smith, S. M., Fox, P. T., Miller, K. L., Glahn, D. C., Fox, P. M., Mackay, C. E., Filippini, N., Watkins, K. E., Toro, R., Laird, A. R., & Beckmann, C. F. (2009). Correspondence of the brain's functional architecture during activation and rest [Number: 31]. *Proceedings of the National Academy of Sciences*, *106*(31), 13040–13045. https://doi.org/10.1073/pnas.0905267106

Smyser, C. D., Inder, T. E., Shimony, J. S., Hill, J. E., Degnan, A. J., Snyder, A. Z., & Neil, J. J. (2010). Longitudinal Analysis of Neural Network Development in Preterm Infants. *Cerebral Cortex*, *20*(12), 2852–2862. https://doi.org/10.1093/cercor/bhq035

Smyser, C. D., & Neil, J. J. (2015). Use of resting-state functional MRI to study brain development and injury in neonates. *Seminars in Perinatology*, *39*(2), 130–140. https://doi.org/10.1053/j.semperi.2015.01.006

Thomas Yeo, B. T., Krienen, F. M., Sepulcre, J., Sabuncu, M. R., Lashkari, D., Hollinshead, M., Roffman, J. L., Smoller, J. W., Zöllei, L., Polimeni, J. R., Fischl, B., Liu, H., & Buckner, R. L. (2011). The organization of the human cerebral cortex estimated by intrinsic functional connectivity. *Journal of Neurophysiology*, *106*(3), 1125–1165. https://doi.org/10.1152/jn.00338.2011

Toulmin, H., Beckmann, C. F., O'Muircheartaigh, J., Ball, G., Nongena, P., Makropoulos, A., Ederies, A., Counsell, S. J., Kennea, N., Arichi, T., Tusor, N., Rutherford, M. A., Azzopardi, D., Gonzalez-Cinca, N., Hajnal, J. V., & Edwards, A. D. (2015). Specialization and integration of functional thalamocortical connectivity in the human infant. *Proceedings of the National Academy of Sciences*, *112*(20), 6485–6490. https://doi.org/10.1073/pnas.1422638112

Williams, L. Z. J., Fitzgibbon, S. P., Bozek, J., Winkler, A. M., Dimitrova, R., Poppe, T., Schuh, A., Makropoulos, A., Cupitt, J., O'Muircheartaigh, J., Duff, E. P., Cordero-Grande, L., Price, A. N., Hajnal, J. V., Rueckert, D., Smith, S. M., Edwards, A. D., & Robinson, E. C. (2021, October 13). *Structural and functional asymmetry of the neonatal cerebral cortex* (preprint). Neuroscience. https://doi.org/10.1101/2021.10.13.464206

Yeo, B. T., Krienen, F. M., Sepulcre, J., Sabuncu, M. R., Lashkari, D., Hollinshead, M., Roffman, J. L., Smoller, J. W., Zöllei, L., Polimeni, J. R., Fischl, B., Liu, H., & Buckner, R. L. (2011). The organization of the human cerebral cortex estimated by intrinsic functional connectivity. *Journal of Neurophysiology*, *106*(3), 1125–1165. https://doi.org/10.1152/jn.00338.2011

Yu, X., Ferradal, S., Dunstan, J., Carruthers, C., Sanfilippo, J., Zuk, J., Zöllei, L., Gagoski, B., Ou, Y., Grant, P. E., & Gaab, N. (2022). Patterns of neural functional connectivity in infants at familial risk of developmental dyslexia. *JAMA Network Open*, *5*(10), e2236102. https://doi.org/10.1001/jamanetworkopen.2022.36102

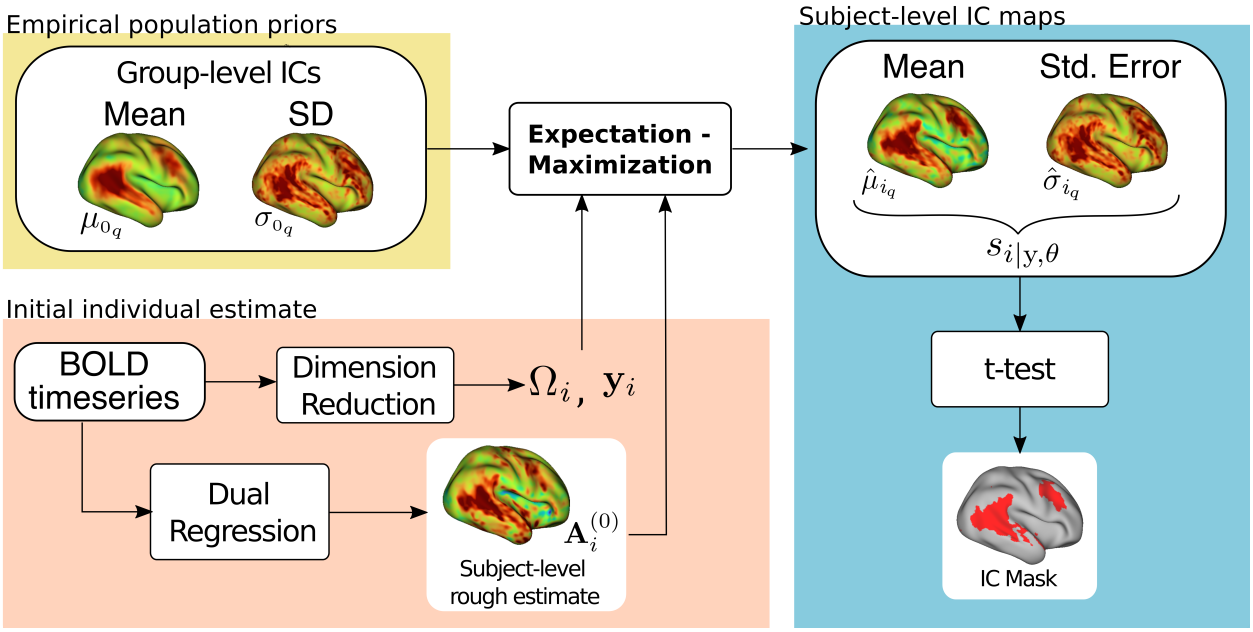

Figure 1: **Estimation of subject-level IC maps**. To estimate the posterior mean and variance of the subject-level ICs, along with the model parameters including the mixing matrix and residual variance, a computationally efficient expectation-maximization (EM) algorithm is used. An initial estimation of the model parameters ($\mathbf{\Omega_i}$) is obtained from dimensionality reduction ($\mathbf{y_i}$) of the BOLD timeseries, while the mixing matrix ($\mathbf{A_i^{(0)}}$) is obtained from a rough dual regression estimate of the individual IC maps. The empirical population priors, namely, the mean ($\mu_\mathbf{0}(\mathbf{v})$) and the between-subject variance $\sigma_\mathbf{0}(\mathbf{v})$ of the group-level IC maps are calculated from a uniform sample of the cohort. After the EM algorithm converges, an estimate of the subject-level mean ($\hat{\mu}_{i_\mathbf{q}}(\mathbf{v})$) and variance ($\hat{\sigma}_{i_\mathbf{q}}(\mathbf{v})$) for each IC is obtained. A binary mask of significant engagement for each IC is obtained from a t-test on the individual mean and variance IC maps.

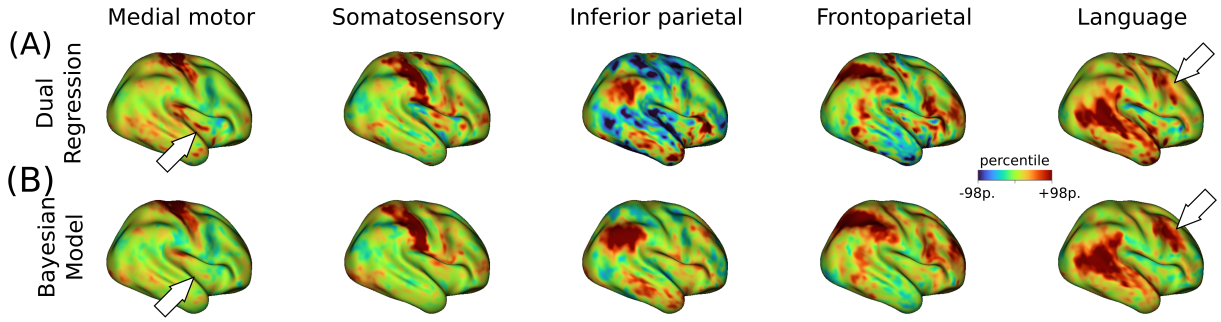

Figure 2: **Subject-level maps obtained from 10 minutes of resting-state fMRI data**. (A) Five representative IC maps obtained from dual regression for a term-born infant scanned at 42.6 weeks PMA. (B) Posterior mean IC maps derived from the Bayesian model produced cleaner maps than the dual regression approach. Note, for example, the more delineated frontal cluster within the language network (white arrows). All maps are projected onto the inflated 40-week atlas.

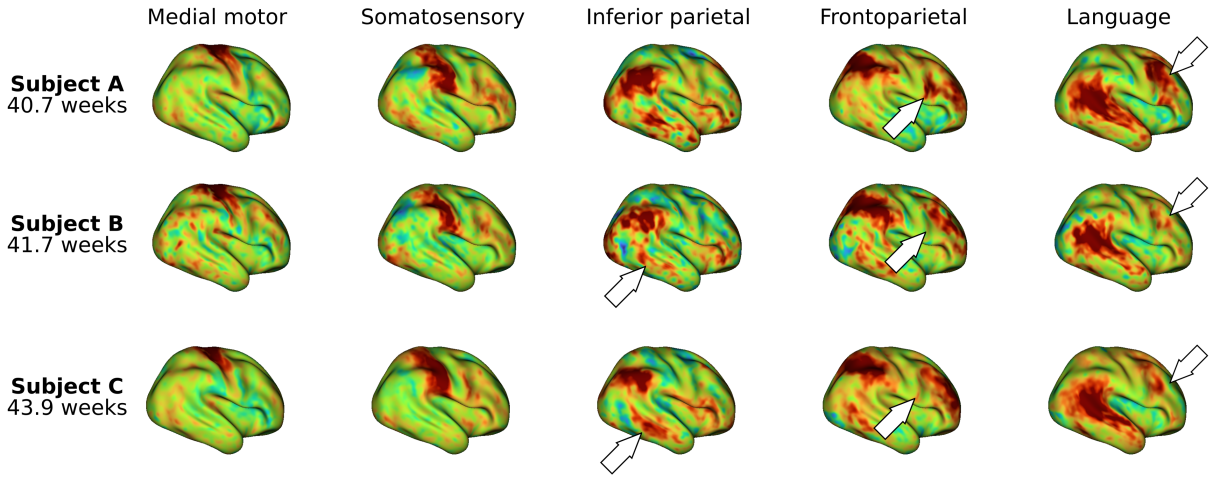

Figure 3: **Subject-level maps across different subjects**. Unthresholded t-statistic maps were computed from the mean and standard error maps derived from the Bayesian model estimation. The five ICs shown in Figure 2 are displayed for three term-born infants scanned at 40.6 weeks PMA, 41.7 weeks PMA, and 43.9 weeks PMA, respectively. Although a general spatial topology is preserved within each specific network, there are evident variations across individuals (as indicated by the white arrows).

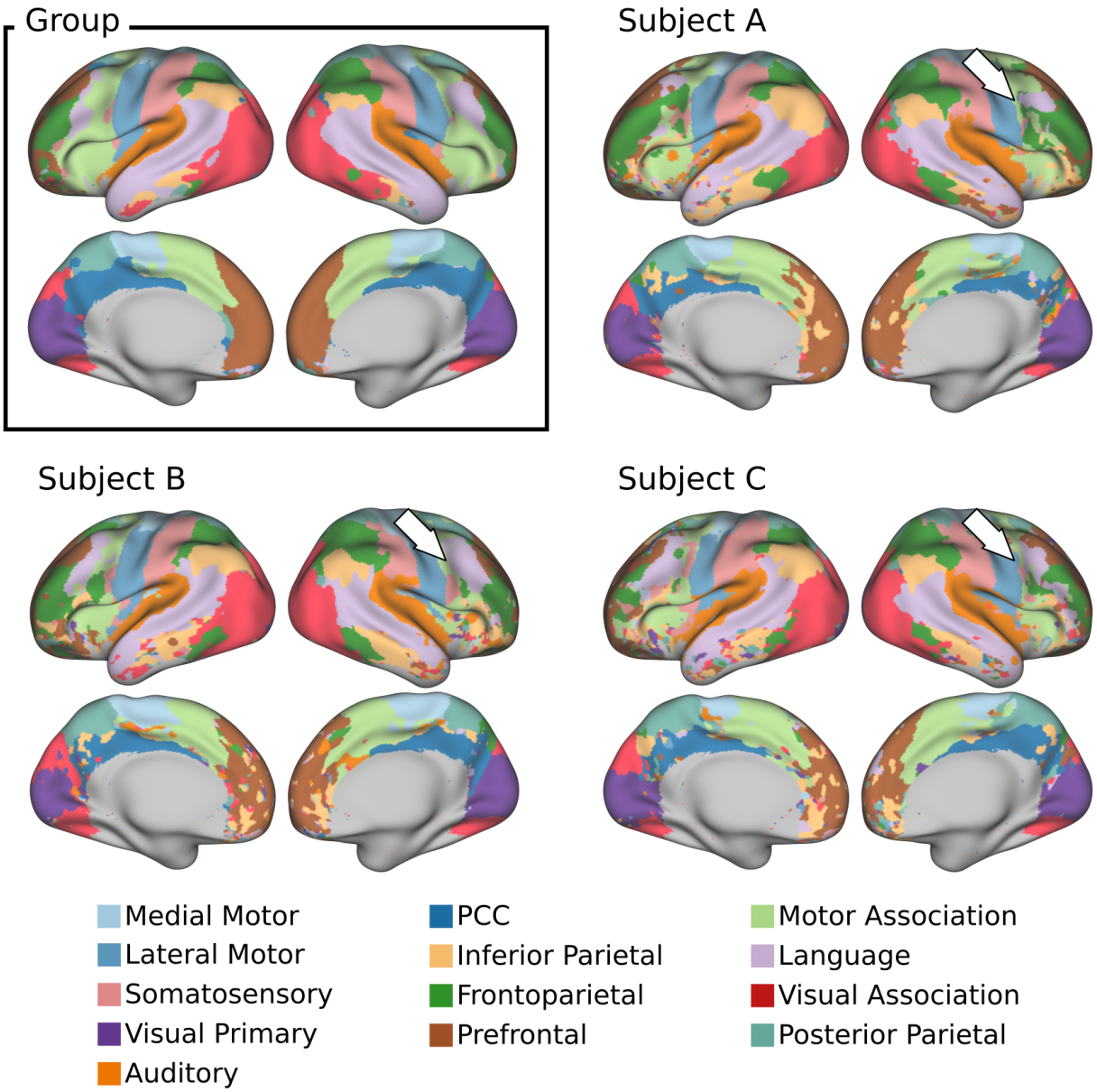

Figure 4: **Group vs. individual parcellations**. Functional parcellations were obtained using a winner-takes-all approach, dividing the cortex into thirteen distinct brain networks and subnetworks. The group parcellation was obtained from the Z-score maps derived from the group ICA analysis on 24 subjects. The individual parcellations were obtained from the subject-level t-maps derived from the Bayesian estimation on the subjects shown in Figure 3. The results are displayed only in regions where the global signal-to-noise ratio (SNR) is greater than 17 dB (see Figure S3 for a whole depiction of the global SNR computed for this cohort).

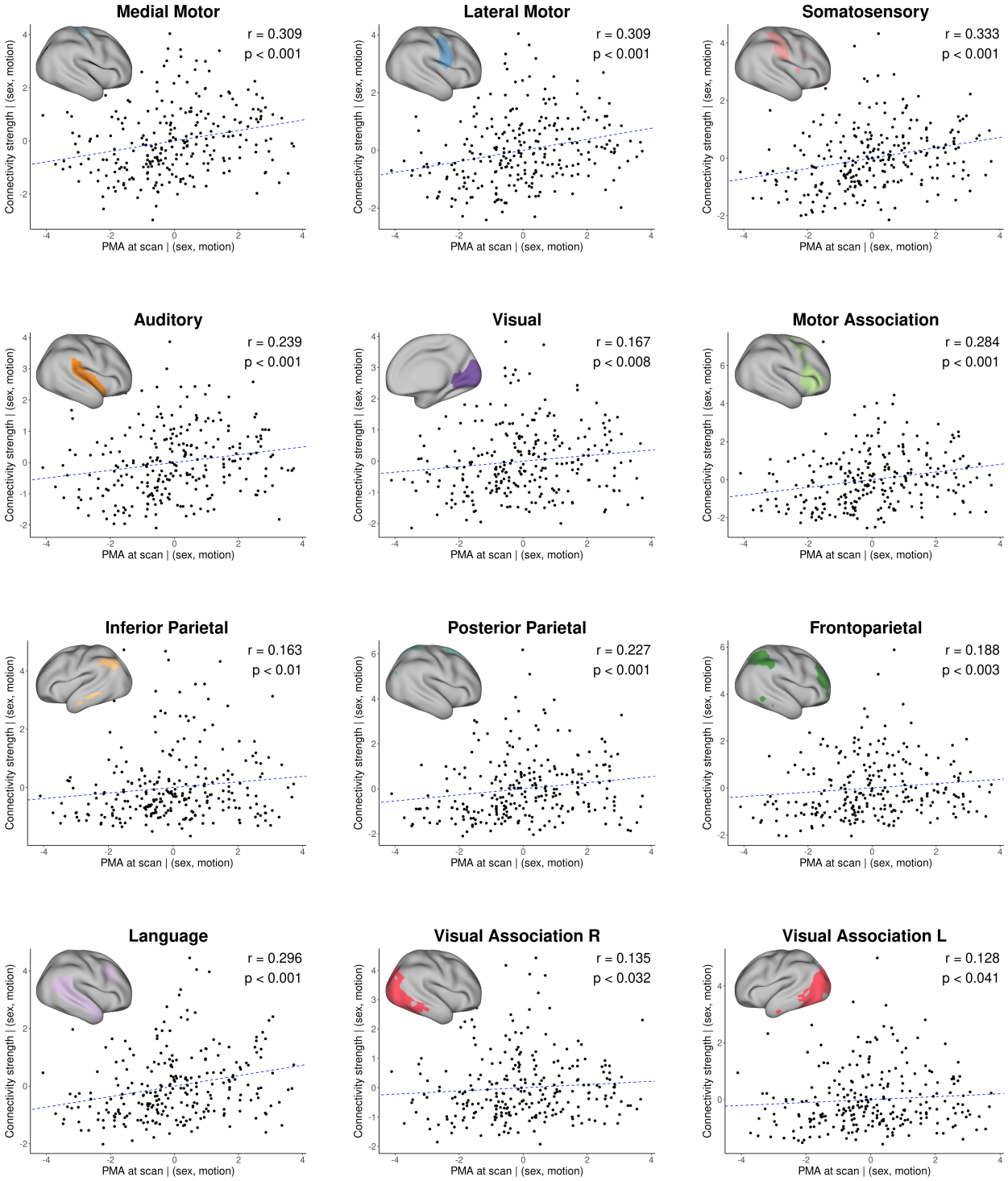

Figure 5: **Effect of age at scan**. The relationship between age at scan and individual connectivity strength for each network was assessed by a Spearman's rank correlation test, after controlling for sex and motion. Networks exhibiting significant effects with age ($p < 0.05$) are shown with Spearman's r and p-values. A dashed blue line showing a linear trend is also included for illustration purposes.

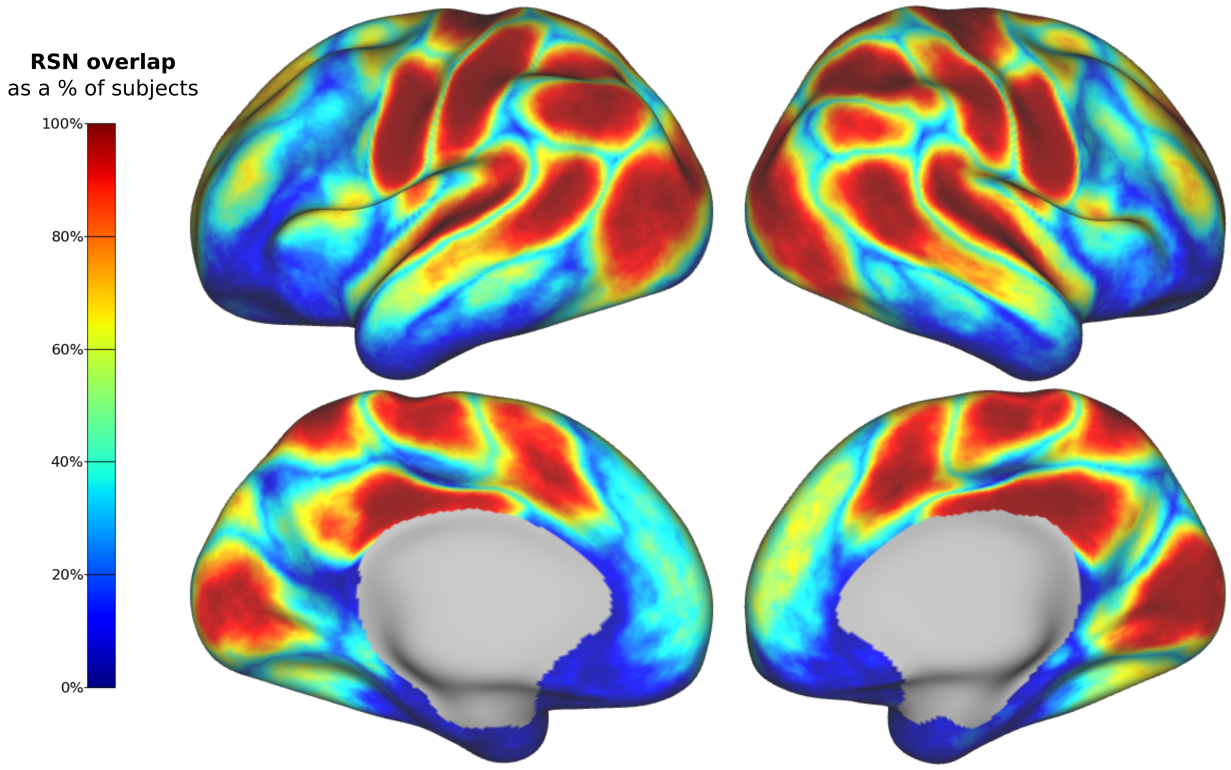

Figure 6: **Frequency map of the entire cohort**. Each vertex represents the percentage of subjects that share the same parcel or network. Networks with higher spatial overlap such as the primary sensory RSNs are represented by warm colors. Note that boundaries between networks and areas with low SNR show higher variability (i.e., low spatial overlap) across subjects.